RSC Advances

ROYAL SOCIETY OF CHEMISTRY

www.rsc.org/advances

RSC Advances

RSCPublishing

COMMUNICATION

Centrifuge-Based Stepwise Chemical Loading Disc for the Production of Multiplex Anisotropic Metallic Nanoparticles

Cite this: DOI: 10.1039/x0xx00000x

Received 00th January 2012,
Accepted 00th January 2012

DOI: 10.1039/x0xx00000x

www.rsc.org/

Byung Hyun Park, Ji Hyun Lee, Jae Hwan Jung, Seung Jun Oh, Doh C. Lee, and Tae Seok Seo*

We have proposed a novel rotary microdevice in which multiplex anisotropic metallic nanoparticles (NPs) can be synthesized under diverse conditions in a high-throughput manner. In this study, by tuning the concentration of ascorbic acid (AA) as a control solution, the shape evolution from hexagon to tripod of gold nanoparticles (Au NPs) was achieved.

Anisotropic metal NPs have been extensively explored for their size- and shape-dependent optical and electrical properties, and their unique intrinsic characteristics render them suitable for a variety of applications in the fields of biomedical sensors,[1,2] nano-electronics,[3] and chemical catalysis.[4-7] Since the anisotropy of metal NPs determines their distinct properties, the fine controllability of the NPs in terms of size and shape is critically required. Anisotropic crystallization processes consist of multiple steps for the seed formation and growth reaction; in these steps, the sequential and programmed reagent loading is of great importance. However, the current state-of-the-art method for optimizing the crystallization process relies on a trial-and-error approach that employs parallel and combinatorial mixing of chemical reagents in a particular sequence at flask scale.[8-12] Such a conventional process for optimizing the anisotropy of nanomaterials is tedious, time-consuming, and complicated. In addition, the large-scale bulk solution-phase synthetic procedure suffers from inhomogeneous reaction conditions, sensitive kinetics, and inconsistent reagent loading. To overcome these limitations and to perform simultaneous screening studies of multiple crystallization conditions in an automated way, a novel practical synthetic platform is necessary. Recently, microfluidics technology has demonstrated its high performance for synthesizing a wide variety of nanoparticles including Au, Pd, CdS, CdSe, CdTe, InP, and FeMn,[13-20] as well as complicated nanostructures such as core/shell CdTe/ZnS quantum dots, 3D graphite microball-Fe_3O_4 nanoparticle hybrids, and Fe_3O_4@metal organic frameworks.[21-23] The advantages of the microfluidics technology include automation, controllable operation capability, rapid mass and heat transfer due to low volumetric dimension, efficient screening for specific parameters with enhanced reproducibility, low reagent consumption, and high integration with *in-situ* characterization.

In general, continuous-flow or droplet-based microdevices have been adopted for producing multiplex nanomaterials under various reaction conditions.[24,25] However, these microfluidic systems require complicated microfabrication steps for high-throughput NPs synthesis and involve complex tube lines and many external pumps to control the fluidics when carrying out multiple reactions. Thus, there is still room for improvement in attempts to realize an ideal chemical synthetic processor.

Centrifuged-based platforms have shown a great potential for bio chemical reaction under various conditions in a high-throughput manner.[26,27] The fluid manipulation, such as the transporting, mixing, and splitting, can be regulated by simple revolution-per-minute (RPM) control and the fluidic physics of a sophisticated microfluidic design without need of tube lines or external syringe pumps.[28] In addition, the high degree of symmetry in a single device enable the synchronization of multiple reactions. While taking full advantage of the rapidity, consistency, and high-throughput capability of centrifugal microfluidics, we have striven to construct a much simpler and automatic microsystem for synthesizing well-defined multiplex anisotropic NPs by tuning an experimental parameter.

In this study, we demonstrate the production of multiplex anisotropic Au NPs in a novel rotary microfluidic device. The rotary microdevice has the capability of automatic and sequential reagent loading with a defined volume by RPM control. Depending on the concentration of AA, which is used as a mild reducing agent, the multiplex anisotropic Au NPs whose shape is from hexagon to tripod are produced at the same time.

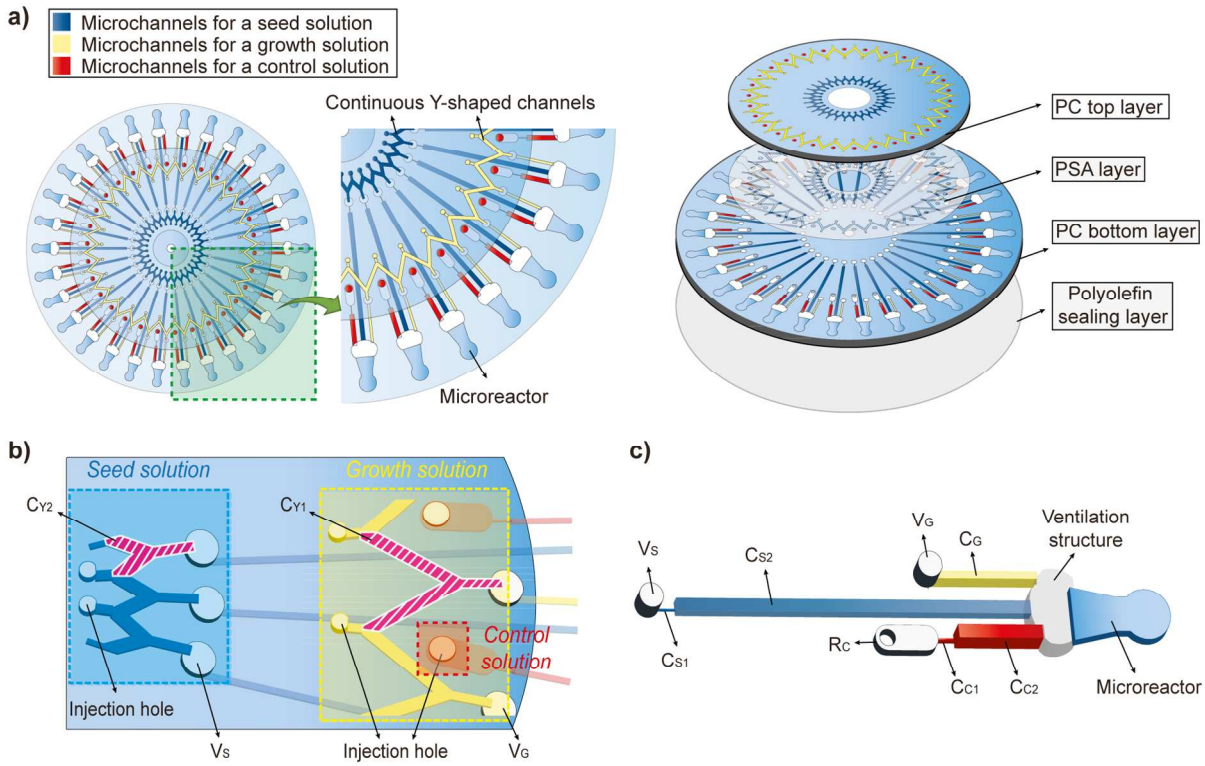

Figure 1. a) The top (left) and tilted dissembled view (right) of the rotary microfluidic device for multiplex anaisotropic Au NP synthesis. Diameters of the top PC and the bottom PC layer were 8 cm and 11.4 cm, and the diameter of a shaft hole was 3.2 cm. The blue, yellow, and red colors represent the seed, growth, and control solutions. b) Schematics of the top PC layer containing the continuous Y-shape microchannels for loading the seed (inner) and growth (outer) solution. C_{Y1} and C_{Y2} are the volumes of a single aliquoting growth and single aliquoting seed solution in the Y-shape microchannel. c) A functional unit in the bottom PC layer is composed of one control solution reservoir (R_C), two via holes (V_S and V_G, for connecting to the seed solution (C_{Y2}) and the growth solution (C_{Y1}), respectively), different dimensional microfluidic channels ($C_{S1,S2}$: seed solution channel, C_G: growth solution channel, $C_{C1,C2}$: control solution channel), a ventilation structure, and a microreactor.

Figure 1a shows the novel high-throughput rotary microdevice used to synthesize thirty different types of Au NPs. The proposed microdevice is composed of four layers (right image of Figure 1a): from top to bottom, 1) a polycarbonate (PC) top layer to identically distribute two reagents into a PC bottom layer; 2) a pressure sensitive adhesive (PSA) layer for bonding the two PC layers; 3) a PC bottom layer that contains the microfluidic channels and 30 microreactors for Au NP synthesis; and 4) a polyolefin sealing layer. Blue, yellow, and red colored areas in the left image of Figure 1a represent the seed solution, the growth solution, and the control solution, respectively. Figure 1b provides a detailed illustration of the PC top layer. The zig-zag continuous channels are adequate for loading a reagent solution in a one shot injection; the dimensions of the Y-shape determine the discrete volumes of the growth solution (dashed area in the outer yellow line, C_{Y1}) and the seed solution (dashed area in the inner blue line, C_{Y2}).[29,30] In this microfluidic design, a centrifugal force causes air blowing from the injection holes to split the liquids in the continuous Y-shaped channels into 30 aliquots, which are delivered to the microreactor chambers in the PC bottom layer through via holes. The split volume of the outer (C_{Y1}) and inner (C_{Y2}) Y-shaped channels can be controlled using the microchannel dimensions. In our case, the calculated volumes of C_{Y1} and C_{Y2} were 6.1 µL and 3 µL, respectively. A representative functional unit of the bottom PC layer is shown in Figure 1c. Each unit consists of one reservoir for the control solution (R_C), two via holes connected with the seed (V_S) and growth (V_G) solutions, an open ventilation structure, and a microreactor. The V_S, V_G, and R_C were linked to the microreactor through different dimensional microfluidic channels (C_{S1} :100 µm width and 150 µm depth, C_{S2} with 1000 µm width and 500 µm depth, C_G with 500 µm width and 800 µm depth, C_{C1} with 100 µm width and 300 µm depth, and C_{C2} with 1000 µm width and 1000 µm depth). The differences in the width and depth of the C_{S1}, C_G, and C_{C1} channels established a unique capillary pressure for each microchannel, so that we are capable of loading the growth solution, the control solution, and the seed solution in sequential order to the microreactor simply by controlling the RPM speed. If the centrifugal pressure induced by the rotation overcomes the capillary pressure of a designated microchannel, the defined solution volumes of C_{Y1}, R_C, and C_{Y2} are released. Once the three solutions were combined together in the microreactor, Au NP synthesis proceeded after gentle shaking. The ventilation structure was patterned to prevent the reagent from flowing backward. The detailed synthetic procedure is described in Table S1.

First, we demonstrated automatic and stepwise solution loading to the microreactor using RPM control. Different colored solutions mimicking the reagents (blue for the seed solution, yellow for the growth solution, and red for the control solution) were prepared. 100 µL of the blue solution and 190 µL of the yellow solution were put into the inner and outer continuous Y-shaped channel through one injection hole, respectively. 5 µL of the red solution was individually introduced into the 30 R_C reservoirs. Then, the sample-loaded

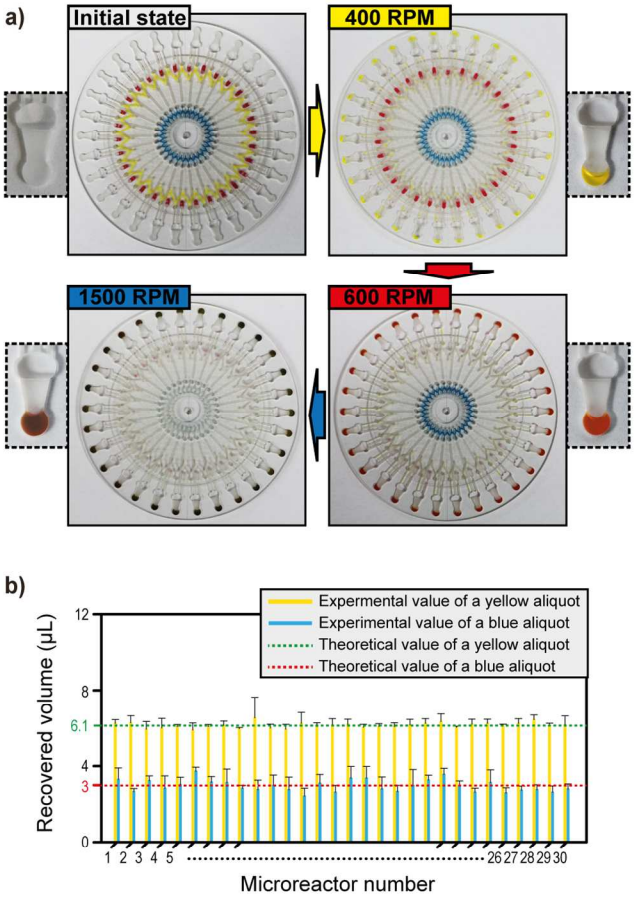

Figure 2. a) Digital images of the rotary microdevice for stepwise reagent loading by RPM control. Through clockwise rotation starting from the top left, the yellow, the red, and the blue solutions were pumped out at 400 RPM, 600 RPM, and 1500 RPM in a sequential order. b) Comparison of the theoretical volume versus the experimentally recovered volume of the yellow and the blue solutions.

microdevice was mounted on the custom-made rotary system so that it could exert centrifugal force by RPM control (Figure S1). As shown in Equation (1), a simple model which balances the centrifugal pressure and the capillary pressure that is given by Young-Laplace equation was adopted to predict the burst RPM in order to eject the specific solution depending on the dimensions of the microfluidic channel.[31]

$$\rho\omega_c^2\bar{r}\Delta r = \gamma\left(\frac{\cos\theta_1+\cos\theta_2}{d}+\frac{2\cos\theta_2}{w}\right) \quad (1)$$

where ρ is the liquid density, $\Delta\boldsymbol{r}$ is the length of the liquid plug, $\bar{\boldsymbol{r}}$ is the mean radial position of the liquid plug, γ is the surface tension of reagents, $\boldsymbol{\theta_1}$ and $\boldsymbol{\theta_2}$ are the respective contact angles of the reagents on the polyolefin sealing layer and on the PC layer, d is the depth of the channel, and w is the width of the channel. From the above balance equation, we could calculate the burst angular velocity ($\boldsymbol{\omega_c}$) and it can be converted into a burst RPM by multiplying a conversion factor (see Table S2 and Table S3 for detailed information). As can be seen in Figure 2a, we gradually increased the RPM in order to load the yellow, the red, and the blue solutions in a consecutive order (see the animation in Video S1-S3). Under the condition of 400 RPM for 10 s, the yellow solution in the outer continuous Y-shaped channel was distributed to 30 aliquots with a volume of C_{Y1} (6.1 μL), each of which was injected into the microreactor through the via hole (See the yellow color in the microreactor). Then, the red solution (5 μL) in the R_C reservoir was pumped out at 600 RPM for 20 s to make the solution color in the microreactor orange (the right bottom image). Finally, the blue solution in the inner continuous Y-shaped channel was split with a volume of C_{Y2} (3 μL) at 1500 RPM for 20 s and dispensed into the microreactor to change the solution color dark purple (the left bottom image). To ensure an equivalent reagent distribution in the microreactors, the collected aliquots of the yellow and the blue solutions were measured using a pipette. Figure 2b shows the theoretical versus the experimental volumes of the yellow and blue aliquots in each microreactor chamber. Compared with the theoretical volumes of C_{Y1} (6.1 μL) and C_{Y2} (3 μL), the gauged aliquot volume of the yellow and blue solutions were 6.1±0.1 μL and 3±0.3 μL, respectively. These results suggest that the proposed microdevice can perform automatic and sequential loading of the chemical reagents by optimizing the microfluidic design and using simple RPM control; the highly uniform distribution of chemical solutions can result in very consistent and reproducible data without the necessity of complex tubing or pumping systems. Therefore, this microsystem will allow us to synthesize anisotropic Au NPs under various conditions in a high-throughput manner with savings of time, cost, and labor.

We set up triplicate reactions for Au NP synthesis with ten different conditions by tuning the concentration of AA and investigated the effect of AA on the morphology change of Au NPs. The seed solution, containing single crystalline Au NPs whose size was 13–17 nm, and the growth solution of $HAuCl_4{\bullet}3H_2O$ and CTAB mixture were prepared by modifying the method in the previous report.[12] An AA solution was used as a control factor by changing its concentration from 0.001 M to 0.2 M. Before introducing the reagents into the reservoirs, the microdevice was exposed to UV ozone for 15 min to produce oxygenous functional groups on the surface of the microreactors, and then, the growth, control, and seed solutions were loaded into the microreactors successively, as described above. As shown in Figure 3a, the spherical seed Au NPs evolved to four categories depending on the concentration of AA: hexagonal shape (0.001 M AA), triangular shape (0.005 M AA), intermediate shape between triangle and tripod (0.01 M ~ 0.15 M AA), and tripodal shape (0.2 M AA). At a low concentration of AA, hexagonal and triangular Au NPs were dominantly formed, showing an edge-biased growth from spherical shape. Theoretically, the AA molecules lose two electrons upon oxidation to reduce Au^{3+} to Au^{+}, but three electrons are needed to fully reduce Au^{3+}. Therefore, the excess of AA is needed for the complete reduction of gold ion.[32] In this study, with an increase of AA concentration, the growth occurred in such a way as to foster the reduction of gold ions in certain facets of the seed particles, leading to a final product of tripodal Au NPs at 0.2 M AA. Figure S2 showed that the color of the Au NPs changed from pink to blue-purple in proportion to the concentration of AA. The shape evolution of the synthesized Au NPs was reflected by the UV-Vis absorption spectra, since variation in the shape or size of the Au NPs which can alter the surface polarization changes the resonant frequency by light (Figure 3b). As the concentration of AA increased, the plasmonic absorption was red-shifted, a sign of the elongation of the Au NPs.[33] While spherical seed particles displayed a 521 nm absorption band, the hexagonal shape Au NPs formed at 0.001 M of AA exhibited a 535 nm absorption band. The peaks at 541 and 543-548 nm resulted from the triangular shape and from the intermediate shape between triangular and tripodal of the Au NPs, respectively, indicating the growth of branches at higher concentrations of AA. For the 0.2 M AA

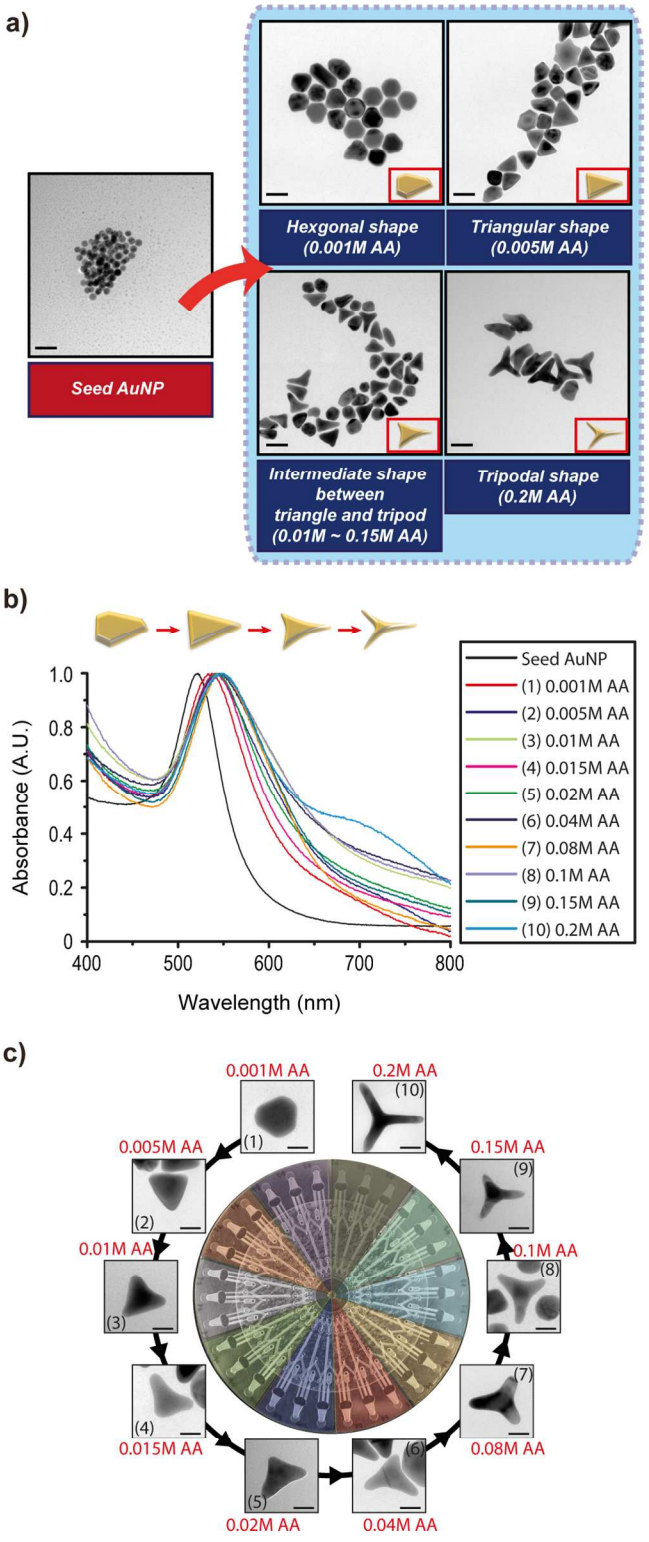

Figure 3. a) Transmission electron microscope (TEM) images of the representative transformed Au NPs that were grown from the 13-17 nm seed Au NPs. Scale bar: 50 nm, b) The UV-Vis absorbance spectra of the Au NP solutions, which show a red-shift in proportion to the AA concentration. c) Representative TEM images showing the shape evolution of the Au NPs. Scale bar: 20 nm

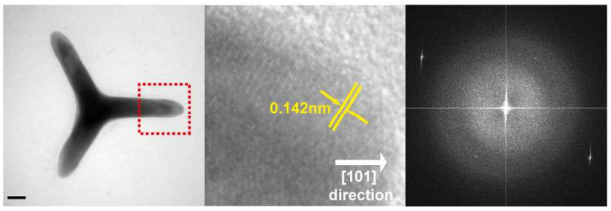

Figure 4. TEM image of the well-developed tripodal Au NP which was synthesized at 0.2 M AA (left, scale bar: 10 nm), a lattice fringe image of the tripodal Au NP (middle), and fast Fourier transform pattern of the middle image (right).

condition, tripodal Au NPs were produced; their absorption spectrum showed a peak at 550 nm and a broad shoulder peak at ~700 nm which is due to the longitudinal plasmonic band. Thus, the absorption spectroscopic analysis corroborates the evolution of elongated Au nanostructures. The systematic shape evolution of Au NPs is illustrated in Figure 3c, which shows representative TEM images of the Au NPs synthesized in ten different synthetic conditions. The transformation of the shape from hexagonal to triangular to tripodal explains the spectroscopic transition observed in the absorption spectra. It should be noted that the simultaneous synthesis of various anisotropic Au NPs using the proposed microdevice can provide a shortcut allowing us to investigate the role of the use of a synthetic parameter in screening for final products with desired shape and morphology without the necessity of using the tedious conventional synthetic processes.

The growth dynamics were examined using a high-resolution TEM. Figure 4 provides an image showing that a tripod-shaped Au NP produced with 0.2 M of AA has three tips whose lengths were each 49 nm. The d-spacing of the lattice plane was measured and found to be ~0.142 nm, meaning that this particle belongs to the (220) plane of gold (JCPDS file no.65-8601). In addition, three tips were extended in <110> directions to form a tripodal shape without any stacking faults or twins. Considering that a hexagonal Au NP was formed at low AA concentration, this epitaxial growth may be attributed to two factors: the fast reduction of gold ions along <110> directions by AA at high concentration in the presence of oxygenous groups in the microreactors and the simultaneous growth inhibition of {111} and {100} facets by CTAB adsorption.

In our experiments, oxygenous groups such as hydroxyls, carbonyls, and carboxylates on the microreactor surface promoted the reduction of gold ion by AA, leading to the formation of well-developed tripodal structures without the use of sodium hydroxide. X-ray photoelectron spectroscopy (XPS) was performed to determine the composition of the UV ozone treated PC. As can be seen in Figure S3, dramatic augmentation of oxygen 1s was found after UV ozone treatment on the PC layer. The UV ozone treated PC displayed carbon 1s peaks at 284.16 eV for aliphatic/aromatic carbon (45.49%), at 286.00 eV for hydroxyl/ether carbon (27.37%), at 288.01 eV for carbonyl carbon (23.04%), and at 289.57 eV for carboxylate carbon (4.1%). This is in stark contrast to the pristine PC, in which only the major peak is located at 284.16 eV for aliphatic/aromatic carbon (95.42%). The increased oxygen intensity enhanced the oxidation rate of AA,[34] resulting in faster reduction of gold ions an anisotropic branch morphology of the Au NPs. It seems that the role of the oxygenous groups on the surface was equivalent to that of sodium hydroxide in the conventional branched Au NP synthetic method.[35-39] As a control, the same procedure was followed without treatment of UV ozone. In this control case, no shape evolution of the Au NPs, as can be seen in Figure 3a, was observed. These results demonstrate that the surface functional groups can

contribute to the morphology control of Au NPs as chemical reagents in the microreactor where the high surface to volume ratio environment was provided to increase the rate of reaction. Taking advantages of the microreactors in this rotary microdevice, AA, a mild reducing agent, can induce the appropriate reduction of Au^{+} on certain crystal facets to obtain anisotropic Au NPs.

The reproducibility of the Au NP synthesis on the microdevice was confirmed by comparing the UV-Vis absorbance spectra of the triplicate products, which were prepared under identical reaction conditions. Figure S4 shows that the triplicate Au NP solutions produced the same absorbance peak, while the red shift of the peaks, compared to that of the seed Au NP, was equally augmented with increasing AA concentration, suggesting the high reproducibility of Au NP synthesis on a chip.

Conclusions

In conclusion, we have proposed a novel rotary microdevice in which multiplex Au NPs can be synthesized under the diverse conditions in a high-throughput manner. Three chemical reagents can be loaded sequentially using the microfluidic design and RPM control, and the reducing agent-dependent shape evolution of Au NPs was achieved. Automatic, simple, reproducible, and multiplex chemical synthesis on a microdevice can be executed within 2 hr, lessening the labor- and time-consuming process of the conventional method. In addition to these features, high-throughput capability can be expanded by incorporating more functional microunits. To further reduce the manual pipetting steps, a concentration gradient generating microfluidic layer can be integrated with the proposed microdevice. A fully automated centrifugal chemical synthesizer can be realized by combining *in-situ* characterization for on-line monitoring of the crystallization process. We envision that this advanced rotary microdevice will be adopted for high-throughput screening and optimization of diverse chemical and biological reactions.

Acknowledgement

This work was supported by Basic Science Research Program through the National Research Foundation of Korea (NRF) funded by the Ministry of Science, ICT & Future Planning (No. 2014R1A5A1009799), BioNano Health-Guard Research Center funded by the Ministry of Science, ICT & Future Planning (MSIP) of Korea as Global Frontier Project (Grant Number H-GUARD_2013M3A6B2078964), and the KIST Institutional Program (Project No. 2E25192-14-189).

Notes and references

Department of Chemical and Biomolecular Engineering (BK21 plus program) and Institute for the BioCentury, Korea Advanced Institute of Science and Technology (KAIST), 291 Daehak-ro, Yuseong-gu, Daejeon, 305-701, South Korea.

† Electronic Supplementary Information (ESI) available. See DOI: 10.1039/c000000x/

1 C. M. Cobley, J. Chen, E. C. Cho, L. V. Wang, Y. Xia, *Chem. Soc. Rev.*, 2011, **40**, 44–56

2 M. Hu, J. Chen, Z.-Y. Li, L. Au, G. V. Hartland, X. Li, M. Marqueze, Y. Xia, *Chem. Soc. Rev.*, 2006, **35**, 1084–1094

3 X. Duan, Y. Huang, Y. Cui, J. Wang, C. M. Lieber, *Nature*, 2001, **409**, 66-69

4 H. Lee, S. E. Habas, S. Kweskin, D. Butcher, G. A. Somorjai, P. Yang, *Angew. Chem. Int. Ed.*, 2006, **45**, 7824–7828

5 A. Mohanty, N. Garg, R. Jin, *Angew. Chem. Int. Ed.*, 2010, **49**, 4962 – 4966

6 R. Narayanan, M. A. El-Sayed, *J. Phys. Chem. B*, 2005, **109**, 12663-12676

7 S. Cheong, J. D. Watt, R. D. Tilley, *Nanoscale*, 2010, **2**, 2045–2053

8 A. Gole, C. J. Murphy, *Chem. Mater.*, 2004, **16**, 3633-3640

9 D. K. Smith, B. A. Korgel, *Langmuir*, 2008, **24**, 644-649

10 Y. Yin, A. P. Alivisatos, *Nature*, 2005, **437**, 664-670

11 C. J. Murphy, T. K. Sau, A. M. Gole, C. J. Orendorff, J. Gao, L. Gou, S. E. Hunyadi, T. Li, *J. Phys. Chem. B*, 2005, **109**, 13857-13870

12 M. R. Langille, M. L. Personick, J. Zhang, C. A. Mirkin, *J. Am. Chem. Soc.*, 2012, **134**, 14542−14554

13 J. Wagner, J. M. Köhler, *Nano Lett.*, 2005, **5**, 685–691

14 S. Duraiswamy, S. A. Khan, *Small*, 2009, **5**, 2828–2834

15 Y. H. Kim, L. Zhang, T. Yu, M. Jin, D. Qin, Y. Xia, *Small*, 2013, **9**, 3462–3467

16 I. Shestopalov, J. D. Tice, R. F. Ismagilov, *Lab Chip*, 2004, **4**, 316–321

17 E. M. Chan, A. P. Alivisatos, R. A. Mathies, *J. Am. Chem. Soc.*, 2005, **127**, 13854–13861

18 S. Yao, Y. Shu, Y.-J. Yang, X. Yu, D.-W. Pang, Z.-L. Zhang, *Chem. Commun.*, 2013, **49**, 7114–7116

19 J. Baek, P. M. Allen, M. G. Bawendi, K. F. Jensen, *Angew. Chem. Int. Ed.*, 2011, **50**, 627–630

20 J. H. Jung, T. J. Park, S. Y. Lee, T. S. Seo, *Angew. Chem. Int. Ed.*, 2012, **51**, 5634–5637

21 R. Kikkeri, P. Laurino, A. Odedra, P. H. Seeberger, *Angew. Chem. Int. Ed.*, 2010, **49**, 2054 –2057

22 D. J. Han, J. H. Jung, J. S. Choi, Y. T. Kim, T. S. Seo, *Lab Chip*, 2013, **13**, 4006–4010

23 M. Faustini, J. Kim, G.-Y. Jeong, J. Y. Kim, H. R. Moon, W.-S. Ahn, D.-P. Kim, *J. Am. Chem. Soc.*, 2013, **135**, 14619−14626

24 H. Wang, K. Liu, K.-J. Chen, Y. Lu, S. Wang, W.-Y. Lin, F. Guo, K.-I. Kamei, Y.-C. Chen, M. Ohashi, M. Wang, M. A. Garcia, X.-Z. Zhao, C. K.-F. Shen, H.-R. Tseng, *ACS nano*, 2010, **4**, 6235–6243

25 P. M. Valencia, E. M. Pridgen, M. Rhee, R. Langer, O. C. Farokhzad, R. Karnik, *ACS Nano*, 2013, **7**, 10671–10680

26 G. Li, Q. Chen, J. Li, X. Hu, J. Zhao, Anal. Chem., 2010, **82**, 4362–4369

27 C. E. Nwankire, M. Czugala, R. Burger, K. J. Fraser, T. M. O'Connell, T. Glennon, B. E. Onwuliri, I. E. Nduaguibe, D. Diamond, J. Ducrée, Biosens. Bioelectron., 2014, **56**, 352–358

28 R. Gorkin, J. Park, J. Siegrist, M. Amasia, B. S. Lee, J.-M. Park, J. Kim, H. Kim, M. Madou, Y.-K. Cho, *Lab Chip*, 2010, **10**, 1758–1773

29 P. Andersson, G. Jesson, G. Kylberg, G. Ekstrand, G. Thorsén, *Anal. Chem.*, 2007, **79**, 4022–4030

30 J. Ducrée, S. Haeberle, S. Lutz, S. Pausch, F. V. Stetten, R. Zengerle, *J. Micromech. Microeng.*, 2007, **17**, S103–S115

31 B. H. Park, J. H. Jung, H. Zhang, N. Y. Lee, T. S. Seo, *Lab Chip*, 2012, **12**, 3875–3881

32 L. Gou, C. J. Murphy, *Chem. Mater.*, 2005, **17**, 3668-3672

33 X. Lu, M. Rycenga, S. E. Skrabalak, B. Wiley, Y. Xia, *Annu. Rev. Phys. Chem.*, 2009, **60**, 167-192

34 M. M. T. Khan, A. E. Martell, *J. Am. Chem. Soc.*, 1967, **89**, 7104–7111

35 S. Chen, Z. L. Wang, J. Ballato, S. H. Foulger, D. L. Carroll, *J. Am. Chem. Soc.*, 2003, **125**, 16186–16187

36 E. Hao, R. C. Bailey, G. C. Schatz, J. T. Hupp, S. Li, *Nano Lett.*, 2004, **4**, 327–330

37 N. Ortiz, S. E. Skrabalak, *Cryst. Growth Des.*, 2011, **11**, 3545–3550

38 A. A. Umar, M. Oyama, *Cryst. Growth Des.*, 2009, **9**, 1146–1152

39 H.-Y. Wu, M. Liu, M. H. Huang, *J. Phys. Chem. B*, 2006, **110**, 19291-19294

We have proposed a novel rotary microdevice in which the multiplex anisotropic Au NPs could be synthesized under the diverse conditions in a high-throughput manner.